Infrared Spectra and Density Functional Calculations for the $Sc(OH)_{2,3}$ and HOScO Molecules and the $Sc(OH)_2^+$ Cation in Solid Argon

Xuefeng Wang and Lester Andrews*

Department of Chemistry, University of Virginia, McCormick Road, P.O. Box 400319, Charlottesville, Virginia 22904-4319

Received: November 10, 2005; In Final Form: December 7, 2005

Reactions of laser-ablated Sc atoms with H_2O_2 molecules or H_2 and O_2 mixtures in excess solid argon gives four major new products, which are identified from concentration dependence, isotopic substitution, the effect of electron trap doping, and comparison to frequencies calculated by the B3LYP density functional. These are the $Sc(OH)_3$ trihydroxide, the $Sc(OH)_2$ dihydroxide, the $Sc(OH)_2^+$ cation, and the trihydroxide anhydride HOScO molecule. The $Sc(OH)_2^+$ cation forms a complex in solid argon that is effectively modeled by calculations for the $[(Ar)_4Sc(OH)_2]^+$ cation including frequency shifts between the neutral and cation dihydroxides. Finally, the $Sc(OH)_4^-$ anion is detected in H_2O_2 experiments.

Introduction

Scandium is a reactive metal, and the reactions of Sc atoms with small molecules such as H_2O, O_2, H_2, and N_2 have been investigated.[1−8] In the matrix-isolation experiments with oxygen, the most noteworthy result is the observation of ScO_2^- and ScO^+ along with ScO,[5] which led to the characterization of noble gas complexes such as $[(Ar)_5ScO]^+$.[9] The Sc reaction with H_2O gives ScO in the gas phase, but the HScOH intermediate is also trapped when the reaction is conducted in solid argon.[1−3]

Recently, we have shown that Group 2 and 4 metal atoms react with H_2O_2 and $H_2 + O_2$ mixtures to form the $M(OH)_2$ dihydroxide molecules, and in the case of Group 4, the tetrahydroxide molecules have also been trapped and characterized.[10−12] Although solid $Sc(OH)_3$ is not as well known as $Ca(OH)_2$, its crystal structure has been characterized as a distorted ReO_3 structure to allow hydrogen bonding between OH groups in different $Sc(OH)_6$ tetrahedra, but pure crystalline Group 4 tetrahydroxides have not been observed.[11−15] However, crystal structures of alkali metal salts of $[Sc(OH)_6]^{3-}$ have been determined.[16] In addition, scandium oxide hydroxide (HO)(ScO) has been prepared in two crystalline modifications.[17]

We report here a matrix-isolation investigation of the Sc and H_2O_2 reaction in order to produce $Sc(OH)_3$ molecules, and we also observe its dehydration product HOScO and the $Sc(OH)_2$ molecule and its cation $Sc(OH)_2^+$. Most interestingly, the latter cation forms an argon complex in the matrix. Successive OH binding energies have been measured in the gas phase and calculated for scandium and other first-row $M(OH)_3^+$ cations.[18−22]

Methods

The laser-ablation matrix-isolation experiment for infrared spectroscopic characterization of new reactive molecules has been described previously.[23] Scandium was co-deposited with H_2O_2 molecules in excess argon onto a 10 K substrate. A Chemglass stopcock containing a urea−hydrogen peroxide complex (Aldrich) provided H_2O_2 molecules to the flowing argon stream and deuterium-substituted urea−D_2O_2 using methods described earlier.[10−12,24,25] Infrared spectra were recorded on a Nicolet 750 spectrometer after sample deposition, after annealing, and after irradiation with a mercury arc lamp (globe removed, full-arc wavelengths > 220 nm). Complementary experiments were conducted with H_2 and O_2 mixtures in order to make straightforward isotopic substitution in the product molecules.[10−12]

Minimum energy structures and harmonic vibrational frequencies of anticipated product molecules were calculated using the B3LYP density functional and the large 6-311++G(3df,3pd) basis set for H and O and the SDD pseudopotential for Sc in the Gaussian 98 program system.[26−28] All geometric parameters were varied, and the converged structures are stable with all real frequencies. Additional MP2 calculations were done for $Sc(OH)_2^+$ and the four argon complex using the SDD pseudopotential for Ar to compare with B3LYP results.

Results

Observations from matrix-isolation experiments and the results of density functional calculations will be presented.

Hydrogen Peroxide. Several experiments were performed with Sc atoms and H_2O_2, and spectra from the most productive experiment are illustrated in Figure 1, and the product absorptions are listed in Table 1. Four bands in the higher frequency O−H stretching region are important, namely, the sharp, strong 3792.6-cm^{-1} band (labeled **tri**), which increases on sample irradiation and annealing at the expense of the weaker 3780.9-cm^{-1} band (labeled **di**), the 3717.8-cm^{-1} feature (labeled **dic**), which increases on full-arc irradiation, and the weak 3750.0-cm^{-1} band (labeled HOScO). Hydrogen peroxide and its photolysis product absorptions common to all laser-ablated metal experiments have been reported previously including the 3730- and 3725-cm^{-1} bands (labeled **c** for HOH−O complex) and weak absorptions for OH and HO_2 radicals.[10−12,25,29,30] The lower-frequency Sc−O stretching region reveals weak ScO^+ and ScO absorptions, new bands at 900.6 and 621.1 cm^{-1} (labeled HOScO), a weak band at 586 cm^{-1} (labeled **a**), and counterparts of the aforementioned species. Similar experiments with lower H_2O_2 concentration or using lower laser energy gave

* To whom correspondence may be addressed. Email: lsa@virginia.edu.

10.1021/jp056518c CCC: $33.50
Published on Web 01/17/2006

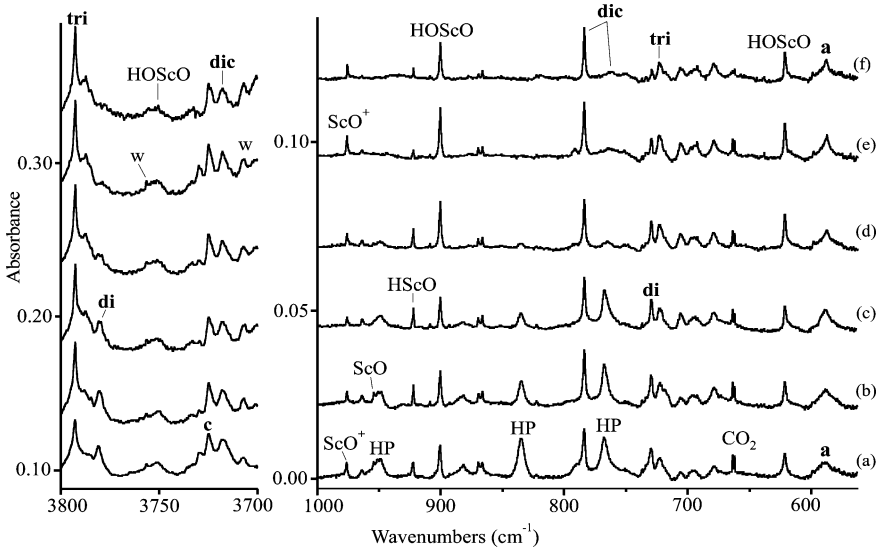

Figure 1. Infrared spectra in the O−H and Sc−O stretching regions for laser-ablated Sc and H_2O_2 reaction products in excess argon at 10 K. (a) Sc and H_2O_2 co-deposited for 60 min, (b) after annealing to 20 K, (c) after >350-nm irradiation, (d) after 240−380 nm-irradiation, (e) after >220-nm irradiation, and (f) after annealing to 30 K. HP denotes bands common to laser-ablated metal experiments with H_2O_2.

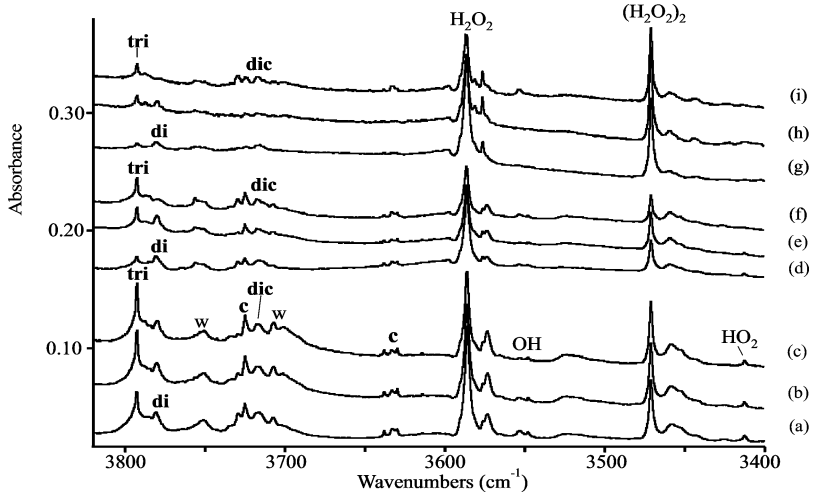

Figure 2. Infrared spectra in the O−H stretching region for laser-ablated Sc and H_2O_2 reaction products using lower reagent concentrations in excess argon. (a) Sc (same laser energy as used for Figure 1 spectra) and H_2O_2 (one-third as much as used for Figure 1 spectra) co-deposited for 60 min, (b) after annealing to 18 K, (c) after annealing to 22 K, (d) Sc (half the laser energy used for Figure 2a) and H_2O_2 (half as much as used for Figure 2a), (e) after annealing to 20 K, (f) after >220-nm irradiation, (g) Sc (one-fourth as much as used for Figure 2a) and H_2O_2 (same as used for Figure 2a), (h) after annealing to 24 K, and (i) after >220-nm irradiation.

TABLE 1: Infrared Absorptions (cm^{-1}) Observed for Products of the Reaction of Sc Atoms and H_2O_2 or $H_2 + O_2$ Molecules

$H_2O_2/H_2 + O_2$	$D_2O_2/D_2 + O_2$	$H_2 + {}^{18}O_2$	$HD + O_2$	$D_2 + {}^{18}O_2$	identification
3792.6/3792.8	2799.6/2798.6	3781.1	3792.6, 2799.6	2779.6	**tri**, $Sc(OH)_3$
3787.3/3787.6	2796.8/2795.5	3775.8	3788.2, 2796.7	2777.7	(di)
/3782.5	2792.6/2792.5	3770.4	3781.5	2774.5	**di**, $Sc(OH)_2$
3780.9/3780.8	2790.5/2790.3	3769.1	2791.2	2772.6	**di**, $Sc(OH)_2$
3750.0/3749.9	2766.4/2766.5	3737.9	3750, 2766.5	2749.5	HOScO
/3723.9	2751.6/2751.5		3721.1	2733.4	**dic**, $Sc(OH)_2^+$
3717.8/3718.0	2744.4/2744.2	3706.5	2747.8	2726.9	**dic**, $Sc(OH)_2^+$
922.4/922.4	921.7/921.7				HScO
900.6/900.8	900.4/900.6	863.3	900.7	863.2	HOScO
784.0/784.0	769.3/769.3	759.7	782.8	744.8	**dic**, $Sc(OH)_2^+$
/776.8	753.5/753.6		761.0	723.8	**dic**, $Sc(OH)_2^+$
729.6/729.6	713.3/713.6	709.8	726	692.4	**di**, $Sc(OH)_2$
723.0/723	697.2/	702.9			**tri**, $Sc(OH)_3$
621.1/621.3	615.0/615.4	598.7	621.3, 615.3	589.0	HOScO
586	569				**a**, $Sc(OH)_4^-$

lower **tri** relative to **di** band yields. Figure 2 compares spectra including the H_2O_2 reagent from experiments with 33 and 20% of the H_2O_2 employed in the experiment shown in Figure 1 using a half and a quarter of the laser energy. Notice that the relative **di** and **tri** band yields are reversed with lower laser energy.

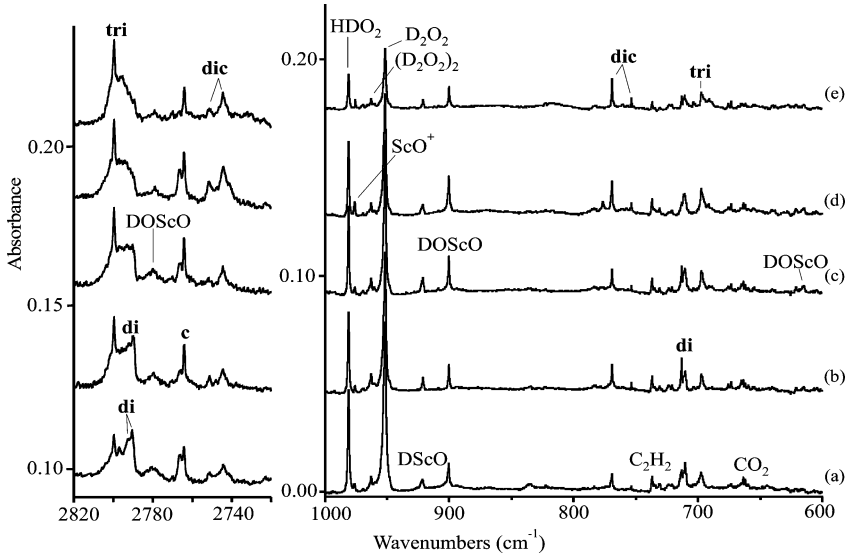

Figure 3. Infrared spectra in the O−D and Sc−O stretching regions for laser-ablated Sc and D_2O_2 reaction products in excess argon at 10 K. (a) Sc and D_2O_2 co-deposited for 60 min, (b) after annealing to 24 K, (c) after 240−380 nm irradiation, (d) after >220-nm irradiation, and (e) after annealing to 30 K.

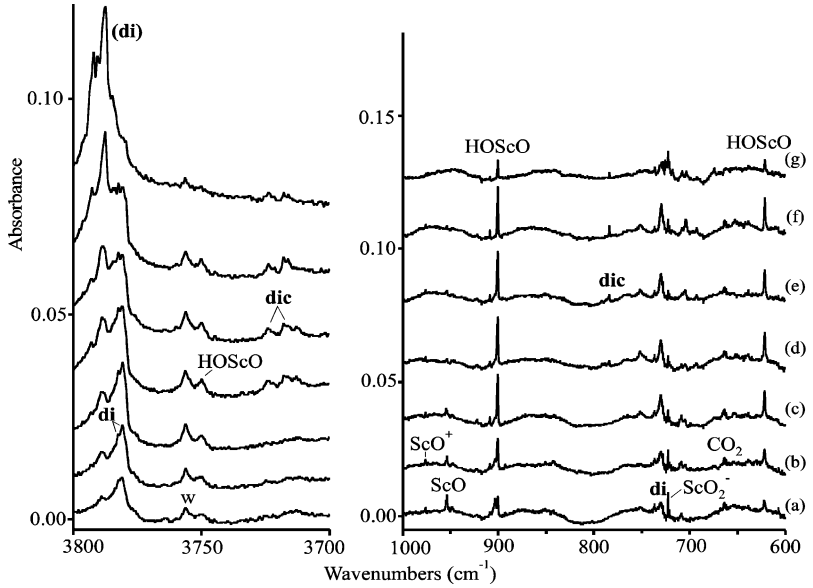

Figure 4. Infrared spectra in the O−H and Sc−O stretching regions for laser-ablated Sc and H_2 plus O_2 reaction products in excess argon at 10 K. (a) Sc and H_2 (3%) and O_2 (0.5%) co-deposited for 60 min, (b) after >350-nm irradiation, (c) after 240−380-nm irradiation, (d) after >220-nm irradiation, (e) after annealing to 16 K, (f) after annealing to 22 K, and (g) after annealing to 30 K.

Spectra from the corresponding D_2O_2 investigation are shown in Figure 3. The upper O−D stretching region exhibits the strong **tri** band at 2799.6 cm^{-1}, two **di** bands at 2792.6, 2790.5 cm^{-1}, a weak DOScO band at 2751.6 cm^{-1}, and two **dic** bands at 2751.6, 2744.4 cm^{-1}, and the lower region illustrates their slightly shifted counterparts. In addition weak bands from hydrogen contamination in the sample were observed at 3793.1 and 3781.6 cm^{-1}, which track the **tri** and **di** deuterium counterparts on photolysis and annealing.

Hydrogen and Oxygen Mixtures. An extensive series of scandium reactions with H_2 and O_2 mixtures was investigated using similar laser-ablation conditions, and the product spectra are given in Figure 4. The strongest initial 3780.8-cm^{-1} absorption (labeled **di**) has a partially resolved 3782.5-cm^{-1} counterpart. Filtered irradiation and annealing increase then decrease the **di** bands and produce a strong new 3787.6-cm^{-1} absorption (labeled **(di)**) and a weak **tri** band at 3792.8 cm^{-1}. Full-arc irradiation produces the **dic** absorption at 3718.0 cm^{-1} and another component at 3723.9 cm^{-1} now observable owing to the absence of the H_2O_2 photolysis product complex.[10−12,25] In the Sc−O stretching region, the 784.0 cm^{-1} **dic** band also exhibits a weak 776.8-cm^{-1} counterpart now observable due to the absence of the broad 767-cm^{-1} band common to H_2O_2 experiments. Of course ScO^+ and ScO bands are stronger, and $(O_2)ScO$ complex, ScO_2^-, ScH_4^-, and other ScH_2 complexes are observed as reported previously.[4−7]

The advantage of complementary $H_2 + O_2$ reactions is the availability of isotopic reagents, and Table 1 gives the shifted product absorptions. Figure 5 shows the evolution of the isotopically substituted product absorptions in the O−D stretching region. Finally, Figure 6 highlights the Sc−O stretching absorptions for **dic** isotopic species.

Calculations. Density functional calculations were done for anticipated product molecules, and the converged minimum energy structures are illustrated in Figure 7, and calculated harmonic (not scaled) frequencies are listed in Tables 2−6. Observed frequencies for the major product species are also given for comparison. We found using the all-electron basis

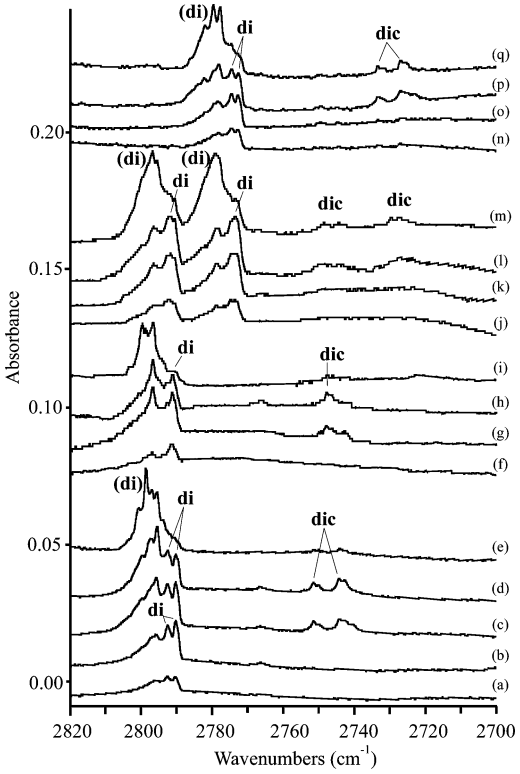

Figure 5. Infrared spectra in the O−D stretching region for laser-ablated Sc and isotopically substituted H_2 and O_2 reaction products in excess argon at 10 K. (a) Sc and D_2 (5%) and O_2 (0.5%) co-deposited for 60 min, (b) after 240−380-nm irradiation, (c) after >220-nm irradiation, and (d) after annealing to 22 K, and (e) after annealing to 30 K. (f) Sc and HD (5%) and O_2 (0.5%) co-deposited for 60 min, (g) after 240−380-nm irradiation, (h) after annealing to 16 K, and (i) after annealing to 30 K. (j) Sc and H_2 and $^{16,18}O_2$ (1% 16−16, 2.5% 16−18, 1.5% 18−18) co-deposited for 60 min, (k) after 240−380-nm irradiation, (l) after >220-nm irradiation, and (m) after annealing to 22 K. (n) Sc and H_2 (5%) and $^{18}O_2$ (0.5%) co-deposited for 60 min, (o) after 240−380-nm irradiation, (p) after >220-nm irradiation, and (q) after annealing to 26 K.

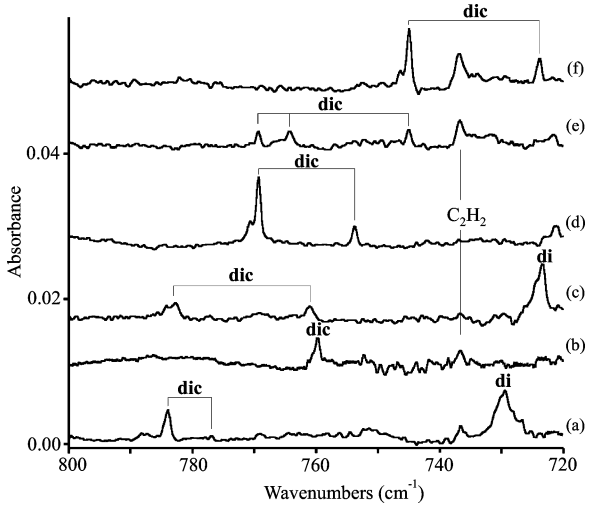

Figure 6. Infrared spectra in the Sc−O stretching region for the Sc reaction product labeled **dic** from isotopic isotopic hydrogen/oxygen mixtures following full-arc irradiation and annealing to 22 K. (a) H_2 and $^{16}O_2$, (b) H_2 and $^{18}O_2$, (c) HD and $^{16}O_2$, (d) D_2 and $^{16}O_2$, (e) D_2 and $^{16,18}O_2$, and (a) D_2 and $^{18}O_2$.

set[26,27] for Sc almost the same frequencies (2−4 cm^{-1} lower) and structure for the $Sc(OH)_2$ ground state. Another 12 kcal/mol higher energy nearly linear, more ionic dihydroxide structure was also located. Starting with one reverse bent Sc−O−H bond (C_1 structure) produced the same C_{2v} minimum-energy structure. We note that our structure for $Sc(OH)_2^+$ is virtually identical to that computed by Ricca and Bauschlicher using a slightly different basis set.[22] Calculations were also performed for argon complexes with the $Sc(OH)_2^+$ cation at both B3LYP and MP2 levels of theory in order to help explain the neutral-to-cation frequency shifts observed here.

Discussion

The new product molecules will be identified from the matrix chemistry, isotopic substitution, and comparison to the results of density functional theory (DFT) frequency calculations.

$Sc(OH)_2$ and $Sc(OH)_3$. The new **di** and **tri** product bands at 3780.8 and 3792.6 cm^{-1} are due to chemically related product species. Our spectra (Figures 1 and 2) show that increasing H_2O_2 concentration and increasing laser energy both favor the **tri** band over the **di** band. These two absorptions are due to O−H stretching modes as the isotopic frequency ratios (H/D = 1.3547 and 1.3550; 16/18 = 1.00309 and 1.00313) attest.[10−12] Hydrogen impurity in the D_2O_2 experiment gave weak slightly shifted 3781.6 and 3793.1 cm^{-1} bands due to partially deuterated products, which therefore must involve more than one O−H group. Although the **di** band yield is about the same in H_2O_2 and $H_2 + O_2$ experiments (compare Figures 1 and 4), the **tri** band yield is much higher with H_2O_2. Furthermore two bands are resolved for these **di** absorptions, which are appropriate for symmetric and antisymmetric stretching modes with little coupling. Spectra for both H_2 and D_2 with $^{16}O_2$, $^{16,18}O_2$, and $^{18}O_2$ produce triplet absorptions for each band, and these are illustrated in Figure 5 for the deuterium system. Note the partially resolved triplets at 2792.6, 2791.7, and 2790.4 cm^{-1} and at 2774.7, 2773.6, and 2772.7 cm^{-1} where the new intermediate bands are clearly due to the two modes of the mixed 16−18 isotopic molecule where both modes of the 16−16 and 18−18 isotopic molecules are observed as with the pure isotopic reagents. These two triplet mixed isotopic absorptions characterize a dihydroxide species with two equivalent O−H subgroups. Our DFT frequency calculations show that the $^{16}O-H$ and $^{18}O-H$ stretching modes of the mixed 16−18 dihydroxide molecule are between the symmetric and antisymmetric stretching modes of the pure isotopic molecules (Table 2). In addition the HD experiment (Figure 5) also gave single 3781.5- and 2791.2-cm^{-1} bands in each region, namely, O−H and O−D stretching, which further indicates that only two O−H (O−D) subgroups are involved in this product species.

The Sc−O stretching region contains **di** and **tri** bands at 729.6 and 723.0 cm^{-1} that track precisely on sample annealing and irradiation with the above O−H stretching modes, respectively. The 16/18 isotopic ratios (1.0279 and 1.0286) are too low for the vibration of a single Sc−O bond, and they are slightly lower than the value for ScO_2^- itself (1.0367)[5] as hydrogen motion is also involved here (the deuterium shift is 19 cm^{-1}). The stronger of these two bands due to the **di** species also exhibits a triplet absorption at 711.0, 705.0, and 690.0 cm^{-1} with stronger intermediate component, which again verifies the participation of two equivalent O atoms.

Assignment of the three **di** bands to the $Sc(OH)_2$ molecule is confirmed by comparison with the calculated frequencies. First, the symmetric and antisymmetric O−H stretching modes are predicted to be strong, with the symmetric mode higher by 1.5 cm^{-1} and 75% as strong as the antisymmetric stretching mode. Our two 3782.5- and 3780.8-cm^{-1} bands agree with this prediction. The third strong band is computed to be the antisymmetric Sc−O stretching mode at 728.9 cm^{-1}, and our

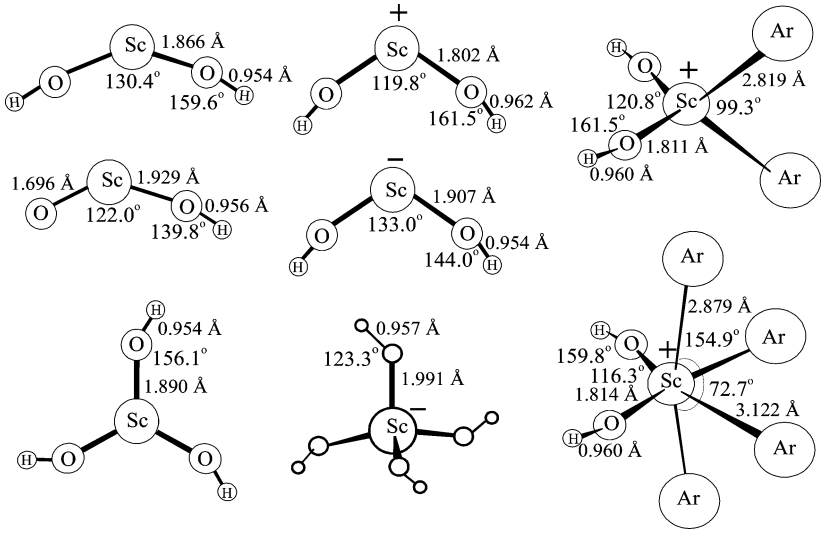

Figure 7. Structures optimized at the B3LYP/6-311++G(3df,3pd)/SDD level of theory for scandium hydroxide species.

TABLE 2: Observed and Calculated Frequencies (cm^{-1}) for $Sc(OH)_2$ in the C_{2v} Structure $^2A_1$ Ground State

	$Sc(OH)_2$		$Sc(OH)(OD)$		$Sc(OD)_2$		$Sc(^{16}OH)(^{18}OH)$		$Sc(^{18}OH)_2$		$Sc(^{18}OD)_2$	
mode	obsd[a]	calcd[b]	obsd	calcd	obsd	calcd	obsd	calcd	obsd	calcd	obsd	calcd
O−H stretch	3782.5	3964.1 (a_1, 154)[c]	3781.5	3963.3 (177)	2792.5	2890.2 (109)	3780.9	3963.4 (176)	3770.4	3950.6 (147)	2774.5	2870.9 (101)
O−H stretch	3780.8	3962.6 (b_2, 200)	2791.2	2889.0 (130)	2790.3	2887.8 (150)	3769.1	3949.9 (171)	3769.0	3949.3 (190)	2779.7	2968.9 (139)
Sc−O stretch	729.6	728.9 (b_2, 224)		723.0 (227)	711.0	714.3 (236)		720.4 (211)	709.8	705.3 (206)	690.0	692.5 (220)
Sc−O stretch		681.3 (a_1, 96)		670.5 (90)		662.6 (77)		662.7 (98)		650.6 (92)		633.9 (73)
Sc−O−H bend		364.5 (a_1, 13)		354.6 (101)		285.8 (51)		362.4 (78)		360.0 (76)		280.2 (49)
Sc−O−H bend		351.3 (a_2, 0)		344.7 (88)		262.1 (108)		350.3 (2)		349.1 (0)		258.9 (0)
Sc−O−H bend		341.0 (b_2, 135)		269.2 (68)		261.8 (0)		339.6 (134)		338.5 (134)		257.8 (105)
Sc−O−H bend		337.9 (b_1, 187)		262.0 (59)		255.9 (72)		336.2 (183)		334.6 (184)		252.8 (70)
O−Sc−O bend		116.2 (a_1, 0)		110.9 (0)		105.9 (0)		114.4 (0)		112.6 (0)		103.5 (0)

[a] Observed **di** bands in solid argon. [b] Calculated at the B3LYP/6-311++G(3df,3pd)/SDD level. [c] Mode symmetry in C_{2v}, infrared intensity, km/mol.

TABLE 3: Observed and Calculated Frequencies (cm^{-1}) for $Sc(OH)_3$ in the C_{3h} Structure $^1A'$ Ground State

	$Sc(OH)_3$		$Sc(OD)_3$		$Sc(^{18}OH)_3$	
mode	obsd[a]	calcd[b]	obsd	calcd	obsd	calcd
O−H stretch		3964.3 (a, 0)[c]		2890.7 (0)		3950.7 (0)
O−H stretch	3792.8	3961.5 (e, 414)	2799.8	2886.6 (318)	3781.1	3948.3 (392)
Sc−O stretch	723.0	722.8 (e, 622)	697.2	707.5 (638)	702.9	700.0 (580)
Sc−O stretch		642.0 (a_1, 0)		621.7 (0)		607.9 (0)
Sc−O−H bend		399.0 (a", 451)		317.2 (311)		394.6 (437)
Sc−O−H bend		377.9 (e", 0)		283.3 (0)		375.4 (0)
Sc−O−H bend		271.9 (e, 414)		227.4 (200)		267.2 (414)
Sc−O−H bend		337.9 (a, 0)		164.5 (0)		217.1 (0)
O−Sc−O bend		157.9 (e, 48)		134.6 (64)		152.6 (40)
O−Sc−O bend		110.3 (a", 8).		99.7 (4)		108.4 (8)

[a] Observed **tri** bands in solid argon. [b] Calculated at the B3LYP/6-311++G(3df,3pd)/SDD level. [c] Mode symmetry in C_{3h}, infrared intensity, km/mol, degeneracy included.

729.6 cm^{-1} band is in good agreement. Even though the calculated O−H stretching mode must be scaled by 0.954 to fit the observed frequency, which is typical for the B3LYP functional,[31] the Sc−O mode fits here without scaling. The weaker symmetric Sc−O stretching mode is not observed.

Our B3LYP calculations predict $Sc(OH)_2$ to be bent at the metal center and slightly bent at the oxygen centers (Figure 7). We expect other low-lying configurations to be important, and indeed we have found a more nearly linear, more ionic structure at 12 kcal/mol higher energy. The $Sc(OH)_2$ molecule is not as ionic as its $Ca(OH)_2$ neighbor based both on Mulliken charges and calculated linear M−O−H structure.[10,32,33] However, the molecule we observe here is nonlinear based on the observed separation and relative intensities of the symmetric and antisymmetric O−H and O−D stretching modes for $Sc(OH)_2$ and $Sc(OD)_2$. In a completely linear dihydroxide molecule the symmetric stretch would be inactive, but here this mode is resolved and has significant intensity. Our calculations for the almost-linear higher energy state predict 0.3- and 1.1-cm^{-1} separations for the symmetric and antisymmetric O−H and O−D stretching modes with only 1% as much intensity for the symmetric mode, but here we observe 1.7- and 2.2-cm^{-1} mode separations and the symmetric counterpart is almost as strong as the antisymmetric mode, which is in agreement with the predicted 1.5- and 2.4-cm^{-1} mode separations and relative intensities for each isotopic modification (Table 2) for the bent $Sc(OH)_2$ structure shown in Figure 7. Furthermore, the natural electron configuration[26] computed for Sc is [core]$4s^{0.69}3d^{0.92}$, which shows substantial valence d orbital participation and helps to rationalize the bent structure. Hence, we believe the bent

TABLE 4: Observed and Calculated Frequencies (cm^{-1}) for $Sc(OH)_2^+$ in the C_{2v} Structure $^1A_1$ Ground State

	$Sc(OH)_2$		$Sc(OH)(OD)$		$Sc(OD)_2$		$Sc(^{16}OD)(^{18}OD)$		$Sc(^{18}OH)_2$		$Sc(^{18}OD)_2$	
mode	obsd[a]	calcd[b]	obsd	calcd	obsd	calcd	obsd	calcd	obsd	calcd	obsd	calcd
O−H stretch	3723.9	3867.1 (a_1, 256)[c]	3721.1	3862.6 (368)	2751.5	2821.8 (155)	2748.6	2817.9(202)		3853.7 (251)	2733.4	2802.4 (149)
O−H stretch	3718.0	3858.1 (b_2, 482)	2747.8	2889.0 (240)	2744.2	2811.8 (323)	2729.8	2796.7 (263)	3706.5	3845.2 (466)	2726.9	2793.3 (304)
Sc−O stretch	784.0	832.8 (b_2, 311)	782.8	827.7 (292)	769.3	816.6 (321)	764.2	809.1 (281)	759.7	804.4 (294)	744.8	790.7 (307)
Sc−O stretch	776.8	808.9 (a_1, 60)	761.0	795.2 (76)	753.6	787.5 (45)		766.2 (78)		774.5 (62)	723.8	755.8 (47)
Sc−O−H bend		488.2 (a_1, 136)		482.4 (201)		382.5 (92)		378.7 (90)		482.4 (131)		374.8 (88)
Sc−O−H bend		485.9 (b_1, 369)		459.6 (148)		374.5 (237)		371.9 (229)		481.5 (362)		368.7 (230)
Sc−O−H bend		478.4 (a_2, 0)		365.3 (102)		356.6 (0)		354.3 (4)		475.4 (0)		352.6 (0)
Sc−O−H bend		402.6 (b_2, 191)		328.2 (115)		301.5 (105)		299.6 (104)		399.8 (190)		297.9 (103)
O−Sc−O bend		160.2 (a_1, 4)		152.6 (3)		145.9 (2)		144.0 (2)		154.8(4)		142.2 (3)

[a] Observed **dic** bands in solid argon. [b] Calculated at the B3LYP/6-311++G(3df,3pd)/SDD level. [c] Mode symmetry in C_{2v}, infrared intensity, km/mol.

TABLE 5: Observed and Calculated Frequencies (cm^{-1}) for HOScO in the Planar $^1A'$ Ground State

	HOScO		DOScO		$H^{18}OSc^{16}O$		$H^{16}OSc^{18}O$		$H^{18}OSc^{18}O$		$D^{18}OSc^{18}O$	
mode	obsd[a]	calcd[b]	obsd	calcd	obsd	calcd	obsd	calcd	obsd	calcd	obsd	Calcd
O−H stretch	3749.9	3923.9 (a, 76)[c]	2766.5	2858.2 (57)		2890.2 (109)	2766.5	3923.9 (76)	3737.9	3910.9 (72)	2779.6	2839.9 (53)
Sc═O stretch	900.8	948.5 (a, 282)	900.6	948.4 (281	900.7	948.4 (284)	863.4	908.7 (267)	863.3	908.6 (268)	863.2	908.6 (267)
Sc−O stretch	621.3	657.8 (a, 96)	615.4	639.7 (189)	598.8	635.2 (138)	621.2	657.5 (153)	598.7	634.8 (135)	589.0	616.8 (171)
Sc−O−H bend		457.8 (a", 141)		356.8 (69)		454.5 (137)		457.6 (140)		454.2 (135)		348.8 (68)
Sc−O−H bend		445.3 (a, 139)		348.6 (108)		438.5 (141)		444.7 (139)		438.0 (141)		343.9 (102)
O−Sc−O bend		171.9 (a, 44)		158.3 (44)		169.9 (44)		167.8 (40)		165.8 (40)		153.6 (39)

[a] Observed **HOScO** bands in solid argon. [b] Calculated at the B3LYP/6-311++G(3df,3pd)/SDD level. [c] Mode symmetry in C_s, infrared intensity, km/mol.

TABLE 6: Observed and Calculated Frequencies (cm^{-1}) for $Sc(OH)_4^-$ with the Approximately S_4 Structure Singlet Ground State

	$Sc(OH)_4^-$		$Sc(OD)_4^-$	
mode	obsd[a]	calcd[b]	obsd	calcd
O−H stretch		3908 (0)[c]		2846 (0)
O−H stretch		3907 (56)		2844 (58)
O−H stretch		3907 (8)		2844 (8)
Sc−O stretch	586	590 (480)	569	570 (600)
Sc−O stretch		566 (169)		556 (246)
Sc−O stretch		538 (0)		528 (0)
Sc−O−H bend		434 (245)		338 (142)
Sc−O−H bend		433 (0)		337 (99)
Sc−O−H bend		421 (370)		323 (0)
O−Sc−O bend		236 (128)		215 (64)

[a] Observed **a** bands in solid argon. [b] Calculated at the B3LYP/6-311++G(3df,3pd)/SDD level. [c] Infrared intensity, km/mol, degeneracy included. Six real frequencies below 200 cm^{-1} not incluced.

$Sc(OH)_2$ structure represents the molecule we have observed in the argon matrix.

The **tri** bands at 3792.6 and 723.0 cm^{-1} are formed on further reactions of $Sc(OH)_2$ with H_2O_2 or in the initial Sc atom reaction with $(H_2O_2)_2$. The first three figures show how the **tri** product is increased on sample annealing, ultraviolet photolysis, and increasing the H_2O_2 concentration or laser energy to promote further reactions. After UV photolysis and annealing, the $H_2 + O_2$ experiments give a relatively small yield of the **tri** species. The mixed isotopic experiments give doublet absorptions without the resolution required for detailed band analysis of the type that provided a definitive identification of the $Zr(OH)_4$ and $Hf(OH)_4$ molecules.[12] Hence, we present strong chemical evidence that the **tri** species is synthesized from straightforward reaction of the **di** species in these systems.

Our **di** and **tri** bands are formed on annealing in the Sc and H_2O experiments of Zhou et al.,[2] and although the upper bands are weak, they appear in the O−H stretching region on annealing, the **di** band first followed by the **tri** band with their associated 729.6- and 723.0-cm^{-1} bands. The 729.6-cm^{-1} **di** band was observed in the first investigation and assigned to a $H_nSc(OH)_2$ species, and Zhou et al. subsequently proposed $HSc(OH)_2$.[1,2] The $Sc(OH)_2$ molecule is just as likely a product in the earlier works,[1,2] and here we reassign this band accordingly.

DFT calculations predict the $Sc(OH)_3$ molecule to be a stable minimum C_{3h} structure (Figure 7) with strong doubly degenerate O−H stretching mode near the antisymmetric O−H stretching mode for $Sc(OH)_2$ and Sc−O mode 6 cm^{-1} lower. The **tri** bands are in good agreement with the prediction particularly considering the approximations involved at the DFT level of theory and the scandium metal system. All of the evidence supports assignment of the **tri** bands to the $Sc(OH)_3$ molecule, and accordingly this work provides the first observation of a neutral metal trihydroxide molecule.

The new absorption in the O−H stretching region near 3787 cm^{-1} is the strongest product absorption after annealing in the H_2 and O_2 experiments, where metal oxide products are also observed, but it is weak in the H_2O_2 investigations. The $Sc(OH)_2$ molecule is reactive, and in H_2O_2 experiments further reaction proceeds readily, but in H_2 and O_2 samples there is little else for $Sc(OH)_2$ to do on annealing but form reagent complexes as found for both ScO and ScH_2.[4−7] Thus, we believe the 3787-cm^{-1} band is due to a complex of $Sc(OH)_2$ most likely with the oxygen molecule.

$Sc(OH)_2^+$. The **dic** absorptions are formed on deposition of laser-ablated Sc with H_2O_2 and increase on full-arc irradiation, and in the $H_2 + O_2$ experiments better resolved bands appear on full-arc irradiation. Following the example of the $Sc(OH)_2$ molecule, the spectra in Figure 4 show two bands for symmetric and antisymmetric O−H stretching modes at 3723.9 and 3718.0 cm^{-1}. These bands shift to 2751.5 and 2744.2 cm^{-1} with the D_2 reagent (H/D ratios 1.3534 and 1.3549), and single intermediate bands are observed at 3721.1 and 2747.8 cm^{-1} with the HD reagent, which show that two O−H (O−D) groups are involved in this vibrational mode. The deuterium counterparts shift to 2733.5 and 2726.7 cm^{-1} with $^{18}O_2$ (16/18 ratios 1.00658 and 1.00634). The scrambled oxygen isotopic spectrum shows two partially resolved triplet absorptions with new intermediate components at 2748.6 and 2729.8 cm^{-1}, which again identifies the vibration of two equivalent O−D groups.

TABLE 7: Mulliken Charges Calculated for Scandium Hydroxide Species[a]

charge	$Sc(OH)_3$	$Sc(OH)_2$	ScOH	$Sc(OH)_2^+$	$Ar_2Sc(OH)_2^+$	$Ar_4Sc(OH)_2^+$	HScO	HOScO
q(Sc)	1.56	1.08	0.57	1.60	1.26	0.91	1.11	1.21
q(O)	−1.05	−1.05	−1.06	−0.89	−0.90	−0.82	−0.64	−1.04[b]
q(H)	0.53	−0.51	0.49	0.59	0.58	0.59	−0.47	0.49
q(Ar)					0.19	0.17		
q(Ar)						0.11		

[a] Calculated at B3LYP/6-311++G(3df,3pd)/SDD level of theory. [b] Charge on terminal oxygen is −0.66.

The isotopic spectra in Figure 6 show stronger and weaker Sc−O stretching modes at 784.0 and 776.8 cm^{-1}, which shift to 769.3 and 753.6 cm^{-1} on deuterium substitution and exhibit 16/18 ratios 1.0329 and 1.0412 with the deuterium oxygen-18 species at 744.8 and 723.8 cm^{-1} that are expected for the antisymmetric and symmetric stretching modes of a bent O−Sc−O group. Indeed the scrambled oxygen isotopic spectrum reveals one intermediate band at 764.2 cm^{-1} and confirms the antisymmetric vibration of two equivalent O atoms in the **dic** species.

Since previous experiments have revealed positive ions such as ScO^+ in laser-ablated scandium experiments,[5,9] we considered the $Sc(OH)_2^+$ cation as a product in these systems. Doping with electron trapping molecules such as CCl_4 and CBr_4 provides a diagnostic for positive ions because the halocarbon molecules preferentially capture ablated electrons and allow for greater survival of isolated positive ions.[34] We used the bromide here since the chloride masks the 784.0-cm^{-1} product absorption, and we doubled the yield of the **dic** bands on deposition relative to neutral species absorptions as compared to the spectra in Figure 1.

Accordingly, calculations were done for the scandium dihydroxide cation, and the four observed frequencies are compared with calculated values in Table 4, and the B3LYP structure is shown in Figure 7. (The MP2 structure is almost the same with 1.800 and 0.959 Å bond lengths and 123.7 and 168.0° bond angles). The lowest O−H stretching frequency calculated and observed here is for the cation, and our calculations predict the antisymmetric O−H stretching frequency 105 cm^{-1} lower for the cation than the neutral dihydroxide, but we observe it only 63 cm^{-1} lower. The symmetric and antisymmetric O−H stretching mode separation is predicted to increase for the cation to 9.0 cm^{-1}, and we observe these modes 5.9 cm^{-1} apart (1.5 cm^{-1} predicted and 1.7 cm^{-1} observed for the neutral dihydroxide). The symmetric mode is higher, 3723.9 cm^{-1}, and has a lower H/D ratio (1.3534) than the lower 3718.0 cm^{-1} antisymmetric stretching mode with the higher H/D ratio (1.3549) as predicted. Furthermore, the calculations predict the antisymmetric Sc−O stretching modes higher by 104 cm^{-1} for the cation than for the neutral dihydroxide, and we observe this to be 54 cm^{-1} higher. In addition the calculations predict the antisymmetric Sc−O stretching mode to be 23.9 cm^{-1} higher than the symmetric counterpart, and we observe this order with a smaller 7.2 cm^{-1} separation. This mode separation is predicted to increase to 29.1 cm^{-1} for the deuterated species, and we observe the separation as 15.7 cm^{-1}. Our signal-to-noise ratio is not good enough below 500 cm^{-1} to observe the bending modes predicted in this region. Finally, the 3718.0- and 784.0-cm^{-1} frequencies observed for $Sc(OH)_2^+$ in solid argon may be compared to the 3784.6 and 592.4 cm^{-1} values observed for the isoelectronic $Ca(OH)_2$ molecule.[10]

To rationalize the dihydroxide neutral-to-cation frequency shifts, complexes containing two, three, and four argon atoms were calculated with $Sc(OH)_2^+$, which are bound by 13, 16, and 18 kcal/mol total, respectively, using the B3LYP density functional (see Figure 7). For comparison more rigorous MP2 calculations were performed, and the tetra-argon complex is bound by 20 kcal/mol, which is in very good agreement with the B3LYP value. The MP2 structure is nearly the same as that found with B3LYP (the argon to scandium bond distances are 0.04 Å shorter and 0.07 Å longer). Furthermore, basis set superposition error is not a serious problem in calculations of this type as errors of 2−4 kcal/mol have been reported.[35] Of more importance, the B3LYP calculated diagnostic antisymmetric stretching frequencies move with successive argon atoms attached in the direction of the observed neutral−cation differences and diminish the calculated neutral−naked cation differences. [The four-argon complex has calculated antisymmetric stretching modes at 804 and 3885 cm^{-1}, the O−H bond lengths *decrease* by 0.02 Å compared to the isolated cation values, and the Mulliken charge on Sc in the cation (1.60) decreases to 1.26 with two argon atoms attached, to 0.91 with four argon atoms, which is just below that for the neutral molecule (1.08), see Table 7]. Hence, the formation of an argon complex with $Sc(OH)_2^+$ helps to explain the observed neutral−cation frequency shifts. The argon matrix shift (or argon complex shift) on $Sc(OH)_2^+$ is therefore to blue shift the O−H stretching mode and red shift the Sc−O stretching mode so we expect the gaseous $Sc(OH)_2^+$ cation to have strong infrared absorptions near 3690 and 810 cm^{-1}.

In addition to ScO^+, argon complexes with CUO, UO_2, and UO_2^+ have been characterized by matrix-isolation experiments and calculations.[9,36−39] Argon atoms tend to fill the intimate coordination sphere such that a coordination number of six is attained. The present $(Ar)_4Sc(OH)_2^+$ complex is therefore analogous to these previous examples.

In summary, the very good agreement between four strong calculated and observed bond stretching frequencies of the $Sc(OH)_2^+$ cation supports our identification of this cation, which in solid argon is effectively the tetra-argon complex with a total argon binding energy of 18 kcal/mol as calculated by DFT or 20 kcal/mol by MP2 methods. This is the first vibrational spectroscopic observation of a metal dihydroxide cation under any conditions.

$Sc(OH)_4^-$. The observation of cations in the samples prompts a search for anions to maintain charge balance, and indeed ScO_2^- is observed in the oxygen experiments. Although the dihydroxide anion is stable by 16 kcal/mol, the calculated IR intensities are too low for these bands to be observed [607 cm^{-1} (a_1, 0 km/mol), 659 cm^{-1} (b_2, 42 km/mol), 3957 cm^{-1} (a_1, 44 km/mol), 3959 cm^{-1} (b_2, 27 km/mol)] particularly in competition with other major product absorptions in these regions. However, the $Sc(OH)_4^-$ anion is even more stable, and the dihydroxide anion combination with H_2O_2 to form the tetrahydroxide anion is exothermic by 185 kcal/mol. The stable approximately S_4 structure illustrated in Figure 7 is calculated to have a very strong degenerate Sc−O stretching mode at 590 cm^{-1} in a region free of other absorptions. Our H_2O_2 experiments reveal a weak 586 cm^{-1} band, which sharpens on annealing and sample irradiation and shifts to 569 cm^{-1} with D_2O_2. This band is not observed in halocarbon-doped samples as electrons are preferentially captured by the halocarbon guest.[34] We note that the

stable ScH_4^- anion was observed in experiments with H_2, and therefore we assign the weak 586-cm^{-1} band to the stable tetrahydroxide anion $Sc(OH)_4^-$.

HOScO. Three new product absorptions at 3749.9, 900.8, and 621.3 cm^{-1} are observed almost unshifted in H_2O_2 and H_2 plus O_2 experiments, and these bands increase together on irradiation with decreasing wavelengths using both reagents. The strongest of these at 900.8 cm^{-1} is characterized by a very small but definite deuterium shift (0.2 cm^{-1}) and a 16/18 isotopic frequency ratio (1.0434) that is identical to that of ScO itself,[4,5] which characterizes a terminal Sc═O stretching mode just below that for ScO at 954.8 cm^{-1}. The associated 621.3-cm^{-1} band couples more to H motion (deuterium shift of 5.9 cm^{-1}) and exhibits a correspondingly lower 16/18 isotopic frequency ratio (1.0374) from the shift to 598.9 cm^{-1}. The scrambled oxygen isotopic experiment gave absorption pairs at 900.8 and 863.4 cm^{-1} and at 621.2 and 598.8 cm^{-1}, which reveal practically no coupling between the two inequivalent oxygen atoms in this species. The 3749.9-cm^{-1} band is clearly due to the corresponding O−H stretching mode as the shifts to 2766.5 and to 3737.9 cm^{-1} and H/D and 16/18 isotopic frequency ratios (1.3555 and 1.00321) indicate. The HD experiment gave a sharp unshifted 2766.5-cm^{-1} band and 3750-cm^{-1} shoulder on water absorption, which show that there is a single H(D) atom in this new product molecule.

Following this information, a DFT calculation was done for HOScO, the straightforward dehydration product of $Sc(OH)_3$, and the converged structure for the $^1A'$ ground state is shown in Figure 7 and the calculated frequencies are given in Table 5. Notice that the calculated O−H stretching frequency is 39 cm^{-1} below that for $Sc(OH)_2$ and our observed bands differ by 31 cm^{-1}, and the calculated Sc═O and Sc−O stretching modes are slightly higher than the observed values as expected.[31] The oxygen-18 shifts are accurately predicted as is the deuterium shift of the Sc═O stretching mode, but the deuterium shift of the Sc−OH stretching mode is overestimated. All in all, very good agreement between three strong observed and calculated frequencies confirms our observation of the new oxide, hydroxide molecule HOScO.

Reaction Mechanisms. The metal atom reaction with H_2O_2 to form metal dihydroxide molecules is straightforward insertion as found in all of our metal experiments,[10−12,40,41] and reaction 1 is exothermic by 181 kcal/mol at the B3LYP/6-311++G-(3df,3pd)/SDD level of theory. The trihydroxide molecule is formed by reactions 2 and 3. Reaction 2 is 75 kcal/mol exothermic, and it is suggested by the decrease in **di** and increase in **tri** absorptions on sample photolysis. The $Sc(OH)_3$ molecule is stable to dehydration, which is a process endothermic by 74 kcal/mol, and the HOScO molecule is probably formed through decomposition of the energized product of reaction 1.

$$Sc + H_2O_2 \rightarrow Sc(OH)_2 \quad (1)$$

$$Sc(OH)_2 + H_2O_2 \rightarrow Sc(OH)_3 + OH \quad (2)$$

$$Sc + (H_2O_2)_2 \rightarrow Sc(OH)_3 + OH \quad (3)$$

$$Sc(OH)_3 \rightarrow HOScO + HOH \quad (4)$$

$$Sc + H_2O_2 \rightarrow [Sc(OH)_2]^* \rightarrow HOScO + H \quad (5)$$

Laser ablation of scandium metal also produces a small proportion of Sc^+ cations in addition to Sc atoms.[5] This we know from the observation of $Sc^{18}O^+$ at 935.5 cm^{-1} in these experiments with $^{18}O_2$ and the earlier investigation.[5] Accordingly, the Sc^+ insertion reaction 6 follows such as that for the isoelectronic Ca atom.[10]

$$Sc^+ + H_2O_2 \rightarrow Sc(OH)_2^+ \quad (6)$$

Electron capture by $Sc(OH)_2$ gives the $Sc(OH)_2^-$ anion, which is stable by 16 kcal/mol, but combination with another H_2O_2 molecule produces the very stable $Sc(OH)_4^-$ tetrahydroxide anion in a reaction exothermic by 185 kcal/mol.

$$Sc(OH)_2 + e^- \rightarrow Sc(OH)_2^- \quad (7)$$

$$Sc(OH)_2^- + H_2O_2 \rightarrow Sc(OH)_4^- \quad (8)$$

The analogous reactions with H_2 and O_2 are also straightforward as $Sc(OH)_2$ is the major product of reaction 9. The increase in the $Sc(OH)_2^+$ cation on full-arc irradiation most likely arises from photoionization of the neutral molecule with a red matrix shift owing to the stabilization of the $Sc(OH)_2^+$ cation by the argon matrix as an argon complex $[(Ar)_4Sc(OH)_2^+]$. Our DFT calculation predicts the ionization energy of $Sc(OH)_2^+$ as 143 kcal/mol, and a red matrix shift of approximately 5000 cm^{-1} is required for this process to occur in solid argon. We calculate the four argon atom binding energy in the cation as 6400 cm^{-1} (18 kcal/mol), which is near that calculated recently for ScO^+ in solid argon.[9]

$$Sc + (H_2)(O)_2 \rightarrow (H_2)(O) + ScO \rightarrow Sc(OH)_2 \quad (9)$$

$$Sc(OH)_2 + 4Ar + 220\ nm \rightarrow (Ar)_4Sc(OH)_2^+ + e^- \quad (10)$$

Bonding Considerations. Several bonding comparisons can be made with the new species reported here. First, notice the Mulliken charges (Table 6) for the three $Sc(OH)_{1,2,3}$ species are nearly the same for the O and H atoms, but note the increasing charge on the Sc metal center. Hence, Sc provides almost the same electron density stepwise for bonding to each of one, two, or three OH groups. This is also revealed in the natural valence electron configurations on Sc for the three hydroxides, $4s^{1.70}3d^{0.63}$, $4s^{0.60}3d^{0.92}$, and $4s^{0.06}3d^{0.93}$, respectively, which show that Sc 4s electon density supports bonding to the OH ligands. Second, the Mulliken charge on Sc in the $Sc(OH)_2$ molecule (1.08) is substantially less than that on Ca in the $Ca(OH)_2$ molecule (1.56), which is consistent with the linear structure for the more ionic calcium dihydroxide molecule and the slightly bent M−O−H structure for the less ionic scandium dihydroxide molecule[10,32,33] (Figure 7). This difference in bonding and structure appears although the O−H stretching frequencies are almost the same (3784.6 and 3780.8 cm^{-1}, respectively, for the Ca and Sc dihydroxide molecules). We note that DFT calculations have also found ScF_2 and $ScCl_2$ to be nonlinear with flat potential-energy surfaces.[42] Third, the O−H stretching frequency for $Sc(OH)_2^+$ is substantially lower (3718.0 cm^{-1}) than for the neutral $Sc(OH)_2$ molecule, but recall that the 3d4s electron configuration of Sc^+ offers less repulsion for binding of two OH radicals than does the $3d4s^2$ configuration of Sc itself,[43] and the stronger Sc−O bonds in the cation (Figure 7) and higher Sc−O stretching frequencies require charge density from the O−H bonds, which results in weaker O−H bonds and lower stretching frequencies in the cation. Fourth, the Mulliken charge on Sc increases in the $Sc(OH)_2$, HOScO, and $Sc(OH)_2^+$ series and the O−H bond length and stretching frequency decrease.

Conclusions

Laser-ablated Sc atoms react with H_2O_2 to form the $Sc(OH)_2$ and $Sc(OH)_3$ hydroxide molecules, the HOScO dehydration product, and the $Sc(OH)_2^+$ cation.

Calculations show that $Sc(OH)_2$ is bent at the metal center, in contrast to $Ca(OH)_2$ which is essentially linear, and as a consequence both symmetric and antisymmetric O−H stretching modes are observed for $Sc(OH)_2$. Likewise, $Sc(OH)_2^+$ (i.e., the tetra-argon complex here in solid argon) is bent at the metal center, and both symmetric and antisymmetric O−H and Sc−O stretching modes are observed, and this molecular identification is made from isotopic and mixed isotopic substitution. Finally, a weak band is observed for the $Sc(OH)_4^-$ tetrahydroxide anion.

All matrix-isolated molecules form van der Waals complexes with the matrix host, including $Sc(OH)_2$, but the $Sc(OH)_2^+$ cation binds argon more strongly (total 18 kcal/mol calculated for four argon atoms), and calculated frequency shifts in the argon complex are in accord with shifts observed between the dihydroxide neutral and cation in the argon matrix. The $Sc(OH)_3$ molecule, observed here as the first metal trihydroxide molecule to be characterized by vibrational spectroscopy, is formed by further reaction with H_2O_2 and is calculated to have the C_{3h} structure. Dehydration leads directly to HOScO, the trivalent oxide hydroxide, which is a stable molecule and solid compound. Finally, the Mulliken charges on Sc increase in the $Sc(OH)_2$, HOScO, and $Sc(OH)_2^+$ series and the O−H bond lengths and stretching frequencies decrease.

Acknowledgment. We gratefully acknowledge financial support from NSF Grant CHE 03-52487 and the opportunity to examine unpublished spectra from the work in ref 2.

References and Notes

(1) Kaufman, J. W.; Hauge, R. H.; Margrave, J. L. *J. Phys. Chem.* **1985**, *89*, 3547.
(2) (a) Zhang, L.; Dong, J.; Zhou, M. *J. Phys. Chem. A* **2000**, *104*, 8882. (b) Our examination of the 3700−3800-cm^{-1} region of spectra from the work described in a.
(3) Liu, K.; Parson, J. M. *J. Chem. Phys.* **1978**, *68*, 1794.
(4) Chertihin, G. V.; Andrews, L.; Rosi, M.; Bauschlicher, C. W., Jr. *J. Phys. Chem. A* **1997**, *101*, 9085.
(5) Bauschlicher, C. W., Jr.; Zhou, M. F.; Andrews, L.; Tobias Johnson, J. R.; Panas, I.; Snis, A.; Roos, B. *J. Phys. Chem. A* **1999**, *103*, 5463.
(6) Wang, X.; Andrews, L. *J. Am. Chem. Soc.* **2002**, *124*, 7610.
(7) Wang, X.; Chertihin, G. V.; Andrews, L. *J. Phys. Chem. A* **2002**, *106*, 9213.
(8) Chertihin, G. V.; Andrews, L.; Bauschlicher, C. W., Jr. *J. Am. Chem. Soc.* **1998**, *120*, 3205.
(9) Zhao, Y.; Wang, G.; Chen, M.; Zhou, M. F. *J. Phys. Chem. A* **2005**, *109*, 6621.
(10) Wang, X.; Andrews, L. *J. Phys. Chem. A* **2005**, *109*, 2782.
(11) Wang, X.; Andrews, L. *Inorg. Chem.* **2005**, *44*, 7189.
(12) Wang, X.; Andrews, L. *J. Phys. Chem. A* **2005**, *109*, 10689 (Group 4).
(13) Schubert, K.; Seitz, A. *Z. Anorg. Chem.* **1948**, *256*, 226.
(14) Wells, A. F. *Structural Inorganic Chemistry*, 4th ed.; Clarendon Press: Oxford, 1975.
(15) Cotton, F. A.; Wilkinson, G.; Murillo, C. A.; Bochmann, M. *Advanced Inorganic Chemistry*, 6th ed.; Wiley: New York, 1999.
(16) Henning, T. J.; Jacobs, H. *Z. Anorg. Allg. Chem.* **1992**, *616*, 71.
(17) Christensen, A. N.; Jensen, J. S. *Acta Chem. Scand.* **1967**, *21*, 121.
(18) Clemmer, D. E.; Aristov, N.; Armentrout, P. B. *J. Phys. Chem.* **1993**, *97*, 544.
(19) Magnera, T. F.; David, D. E.; Michl, J. *J. Am. Chem. Soc.* **1989**, *111*, 4100.
(20) Crellin, K. C.; Beauchamp, J. L.; Goddard, W. A.; Geribaldi, S.; Decouzon, M. *Int. J. Mass Spectrosc.* **1999**, *183*, 121.
(21) Bauschlicher, C. W., Jr.; Partridge, H. *Chem. Phys. Lett.* **1997**, *272*, 127.
(22) Ricca, A.; Bauschlicher, C. W., Jr. *J. Phys. Chem. A* **1997**, *101*, 8949.
(23) Andrews, L. *Chem. Soc. Rev.* **2004**, *33*, 123 and references therein.
(24) Pettersson, M.; Tuominen, S.; Rasanen, M. *J. Phys. Chem. A* **1997**, *101*, 1166.
(25) Pehkonen, S.; Pettersson, M.; Lundell, J.; Khriachtchev, L.; Rasanen, M. *J. Phys. Chem. A* **1998**, *102*, 7643.
(26) Frisch, M. J.; Trucks, G. W.; Schlegel, H. B.; Scuseria, G. E.; Robb, M. A.; Cheeseman, J. R.; Zakrzewski, V. G.; Montgomery, J. A., Jr.; Stratmann, R. E.; Burant, J. C.; Dapprich, S.; Millam, J. M.; Daniels, A. D.; Kudin, K. N.; Strain, M. C.; Farkas, O.; Tomasi, J.; Barone, V.; Cossi, M.; Cammi, R.; Mennucci, B.; Pomelli, C.; Adamo, C.; Clifford, S.; Ochterski, J.; Petersson, G. A.; Ayala, P. Y.; Cui, Q.; Morokuma, K.; Malick, D. K.; Rabuck, A. D.; Raghavachari, K.; Foresman, J. B.; Cioslowski, J.; Ortiz, J. V.; Stefanov, B. B.; Liu, G.; Liashenko, A.; Piskorz, P.; Komaromi, I.; Gomperts, R.; Martin, R. L.; Fox, D. J.; Keith, T.; Al-Laham, M. A.; Peng, C. Y.; Nanayakkara, A.; Gonzalez, C.; Challacombe, M.; Gill, P. M. W.; Johnson, B.; Chen, W.; Wong, M. W.; Andres, J. L.; Gonzalez, C.; Head-Gordon, M.; Replogle, E. S.; Pople, J. A. *Gaussian 98*, revision A.6, Gaussian, Inc.: Pittsburgh, PA, 1998 and references therein.
(27) Frisch, M. J.; Pople, J. A.; Binkley, J. S. *J. Chem. Phys.* **1984**, *80*, 3265.
(28) Andrae, D.; Haeussermann, U.; Dolg, M.; Stoll, H.; Preuss, H. *Theor. Chim. Acta* **1990**, *7*, 123.
(29) Cheng, B.-M.; Lee, Y.-P.; Ogilvie, J. F. *Chem. Phys. Lett.* **1988**, *109*, 151.
(30) (a) Milligan, D. E.; Jacox, M. E. *J. Chem. Phys.* **1963**, *38*, 2627. (b) Smith, D. W.; Andrews, L. *J. Chem. Phys.* **1974**, *60*, 81.
(31) Scott, A. P.; Radom, L. *J. Phys. Chem.* **1996**, *100*, 16502.
(32) Kaupp, M.; Schleyer, P. v. R. *J. Am. Chem. Soc.* **1992**, *114*, 491.
(33) Ikeda, S.; Nakajima, T.; Hirao, K. *Mol. Phys.* **2003**, *101*, 105.
(34) Andrews, L.; Citra, A. *Chem. Rev.* **2002**, *102*, 885 and references therein.
(35) Diep, P.; Jordan, K. D.; Johnson, J. K.; Beckman, E. J. *J. Phys. Chem. A* **1998**, *102*, 223.
(36) Li, J.; Bursten, B. E.; Liang, B.; Andrews, L. *Science* **2002**, *295*, 2242.
(37) Liang, B.; Andrews, L.; Li, J.; Bursten, B. E. *J. Am. Chem. Soc.* **2002**, *124*, 9016.
(38) Li, J.; Bursten, B. E.; Andrews, L.; Marsden, C. *J. Am. Chem. Soc.* **2004**, *126*, 3424.
(39) Wang, X.; Andrews, L.; Li, J.; Bursten, B. E. *Angew. Chem., Int. Ed.* **2004**, *43*, 2554.
(40) Wang, X.; Andrews, L. *J. Phys. Chem. A* **2005**, *109*, 3849.
(41) Wang, X.; Andrews, L. *Chem. Commun.* **2005**, 4001.
(42) Wang, S. G.; Schwarz, W. H. E. *J. Chem. Phys.* **1998**, *109*, 7252.
(43) Moore, C. E. *Atomic Energy Levels*; National Bureau of Standards, Circular 467: Washington, DC, 1952.